

Supplementary Information

Adhesion of flat-ended pillars with non-circular contacts

Aoyi Luo,^{‡a} Amir Mohammadi Nasab,^{‡b} Milad Tatari,^b Shuai Chen,^{bc}

Wanliang Shan^{*bc} and Kevin T. Turner^{*a}

[‡] Authors have contributed equally.

^a Department of Mechanical Engineering and Applied Mechanics, University of Pennsylvania, 220 South 33rd Street, Philadelphia, Pennsylvania 19104, USA. E-mail: kturner@seas.upenn.edu

^b Mechanical Engineering Department, University of Nevada, Reno, 1664 N. Virginia Street, Reno, Nevada 89557, USA.

^c Department of Mechanical and Aerospace Engineering, Syracuse University, Syracuse, NY 13244, USA. E-mail: washan@syr.edu.

Images of the laser cut Ecoflex-PDMS layer. Fig. S1 shows images of the edge of the laser cut Ecoflex-PDMS layers. Fig. S2 shows the side view of a square laser cut Ecoflex-PDMS layer.

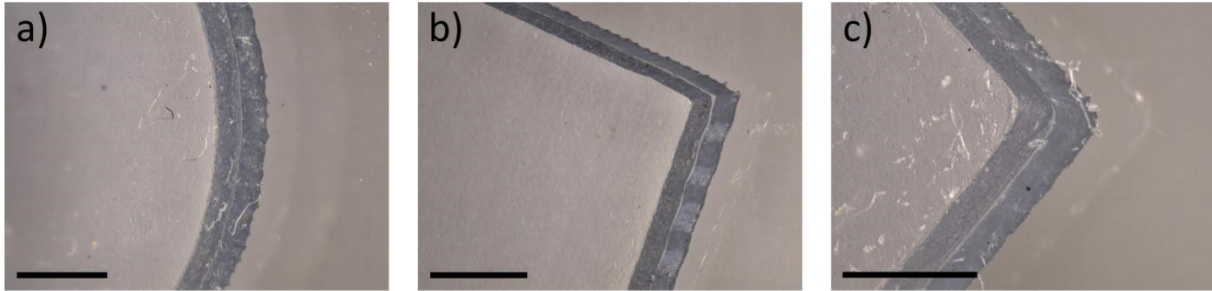


Fig. S1 Extended depth-of-field (EDOF) microscopic images of the edges of circular, square and rectangular laser cut Ecoflex-PDMS layers. The Ecoflex layer is on the top, and the PDMS is on the bottom. The images are taken with a $\sim 23^\circ$ tilt angle. The scale bar is 1 mm.

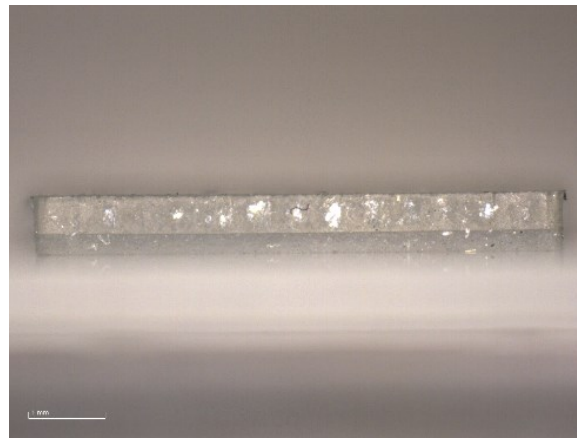


Fig. S2 Optical microscope image of the side view of a square laser cut Ecoflex-PDMS layer. The upper layer is PDMS and the lower layer is Ecoflex.

Linear elastic vs. hyperelastic. Ecoflex is a hyperelastic material and can be described by a Neo-Hookean constitutive model (tensile tests results: $\mu=0.024$ MPa, $\nu=0.499$, $d=0.167$ MPa $^{-1}$). The FE-predicted normal stress distribution at the adhered interface under experimentally measured pull-off load is compared for FE simulations with hyperelastic and linear elastic

constitutive laws. The normal stress distribution within the edge singularity-dominated region for a hyperelastic model no longer takes the form $\sigma_{zz}=Kd^n$ and the value is lower than that predicted by linear elastic model. This may enhance the adhesion strength for homogenous pillars and composite pillars with large t/R ratio where the crack initiates from the edge. However, the stress distribution away from the singularity-dominated region is not significantly affected by the hyperelastic model. The overall trends are the same for hyperelastic and linear elastic models, and it is expected that the adhesion strength achieved by the composite pillars with center and internal crack will not be significantly affected by using a hyperelastic model rather instead of a linear elastic model.

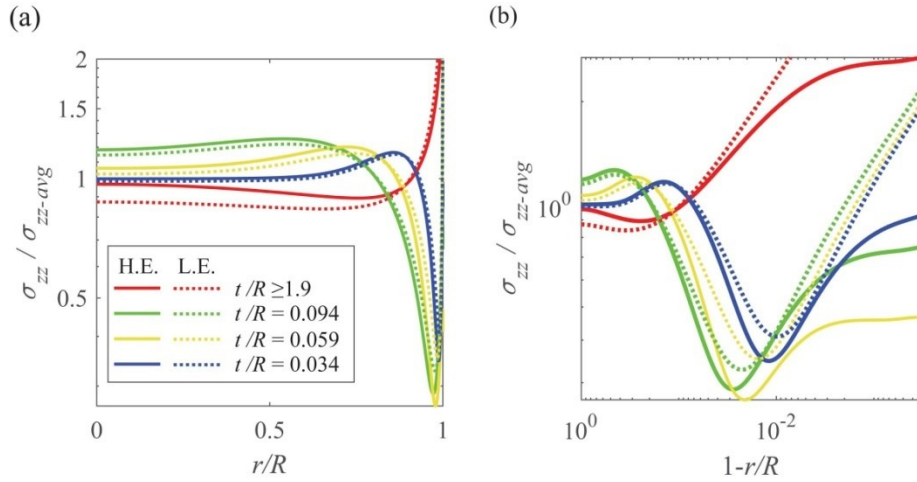


Fig. S3 Normal stress distribution at the adhered interface for composite Ecoflex-PDMS pillars calculated using a hyperelastic model for and a linear elastic model for the Ecoflex layer.

Analysis of the adhesion strength based on fracture mechanics. For a homogenous system, based on linear elastic fracture mechanics¹, the local strain energy release rate at a defect/crack of size a at the interface is given by:

$$G = Y^2 \frac{\sigma_{zz}^2 \pi a}{E_1^*} = Y^2 \frac{\sigma_{zz-avg}^2 \pi a}{E_1^*} \left(\frac{\sigma_{zz}}{\sigma_{zz-avg}} \right)^2 \quad (S1)$$

where Y is a geometry factor that depends on the position of the crack, $E_1^* = E_1/(1-\nu^2)$ is the plane strain modulus, and σ_{zz} is the local stress at the defect/crack. The crack will propagate at the position where G reaches G_c first, and then the adhesion strength σ_{ad} is

$$\sigma_{ad} = \frac{\sqrt{G_c E_1^*}}{\frac{\sigma_{zz}}{\sigma_{zz-avg}} Y \sqrt{\pi a}} \quad (S2)$$

If the crack is away from the edge, $Y=0.47$, which represents a penny-shaped crack at the interface between a rigid substrate and an elastic body.¹ If the crack initiation site is close to the edge, Y becomes larger due to the effect of the free edge. In order to reach high adhesion strength for given material and interface pair (i.e. fixed G_c and E_1^*), $\sigma_{zz}/\sigma_{zz-avg}$ and Y must both be minimized. Thus, it is desirable to have the crack initiate at an internal site away from the edge to obtain a small Y and to keep the peak stress $\sigma_{zz}/\sigma_{zz-avg}$ in the internal region of the contact as low as possible.

The above discussion provides guidance on the design of homogenous pillars. For the composite pillars studied in this work, Y not only depends on the position of the crack, but also depends on the ratio of crack length to tip layer thickness (a/t) and the modulus contrast (E_2^*/E_1^*) due to a heterogeneous toughening effect.²⁻⁵ For a crack away from the edge, when a/t is sufficiently small, the strain energy release rate is⁴

$$G = 0.47^2 \frac{\sigma^2 \pi a}{E_1^*} \quad (S3)$$

This is the same as the aforementioned case of a penny-shaped crack at an interface between a rigid substrate and a homogenous elastic body with modulus E_1^* . However, when a/t is sufficiently large, soft tip behaves as an adhesive layer on the end of the stiff pillar. In the limiting case, the soft layer has a negligible effect on the overall deformation and the strain energy release rate is akin to that of a homogenous stiff pillar with modulus E_2^* :

$$G = 0.47^2 \frac{\sigma^2 \pi a}{E_2^*} \quad (S4)$$

which can be rewritten as:

$$G = \left(0.47 \sqrt{\frac{E_1^*}{E_2^*}} \right)^2 \frac{\sigma^2 \pi a}{E_1^*} \quad (\text{S5})$$

Given $E_2^*/E_1^*=27.8$ in this study, effective Y decreases from 0.47 to 0.09 as a/t increases. Thus, for given a crack length a , smaller t leads to smaller Y , which leads to higher adhesion strength. In summary, for the composite pillar to reach high adhesion strength, it is desirable to have the crack initiated at an internal site away from the edge and the internal peak stress as low as possible, while keeping the tip layer thin. For the circular composite pillars (Fig. 3), the magnitude of stress singularity at edge reduces as t/R reduces and plateaus when $t/R < 0.1$, so for the composite pillar with $t/R=0.06$, the stress at edge is low enough to shift the crack initiation site away from the edge as observed in experiment. Moreover, the composite pillar with $t/R=0.06$ has the lowest internal peak stress among all the t/R investigated. While a further decrease of t/R below 0.06 results in a thinner tip layer and a stronger heterogeneous effect, a higher peak stress is observed and the position of the peak stress moves closer to the edge, which leads to reduction of the adhesion as t/R reduces below 0.06. As a result, the composite pillar with $t/R=0.06$ is observed to have the highest adhesion in experiment.

Stress distributions for circular composite pillars with various elastic modulus ratios. The FE-predicted normal stress distributions at the adhered interface for circular composite pillars with various elastic modulus mismatches are shown. As seen in Fig. S4, the trend of the stress distribution as a function of t/R is similar for different elastic modulus mismatch of the materials, but the value of t/R to reach a specific stress distribution decreases as the elastic modulus mismatch of the materials used increases.

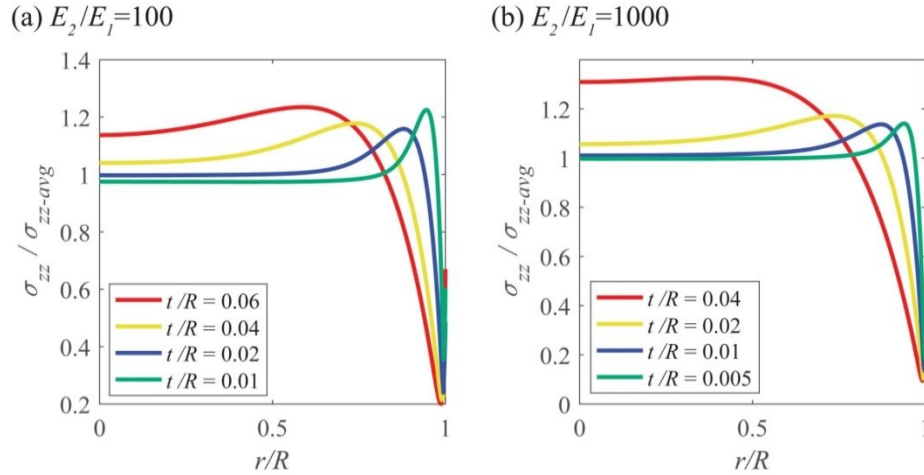


Fig. S4 Normal stress distribution at the adhered interface for pillars with circular cross-section with different t/R ratios: (a) $E_2/E_1=100$. (c) $E_2/E_1=1000$.

Images of the delamination process. A sequence of images are shown here to illustrate how failure progresses at the adhered interface for rectangular pillars with $t/L=0.06$.

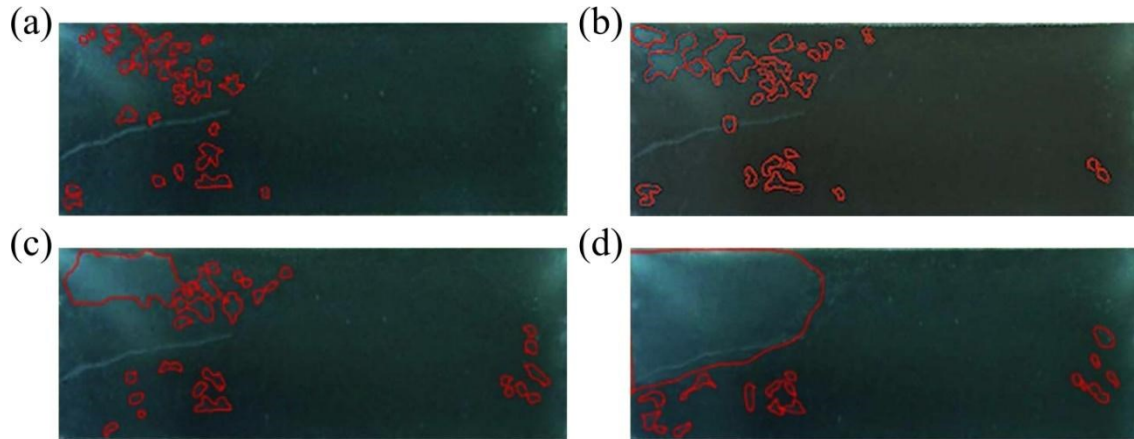


Fig. S5 Original images showing how failure progresses at the adhered interface for rectangular pillars with $t/L=0.06$. Fig. 7 in the paper is obtained from these images. The sequence of images show different time points in the test and were chosen to show (a) nucleation, (b) growth and (c) merging of voids, ultimately resulting in (d) partial detachment and eventual interface failure. The dimensions of the adhered interface shown in each of these images is 8.4×3.5 mm.

Minimum spacing. According to the study from Glassmaker et al.⁶, the minimum edge to edge spacing $2w_s$ required for square pillars to prevent lateral sticking is

$$w_s = \left(\frac{h^4 G_c}{6EL^3} \right)^{1/2} \quad (\text{S6})$$

and the minimum edge to edge spacing $2w_c$ required for circular pillars to prevent lateral sticking is

$$w_c = \left(\frac{h^4 G_c}{6ER^3} \right)^{1/2} \left(\frac{2^{10} G_c}{\pi^4 E^* R} \right)^{1/6} \quad (\text{S7})$$

where h is the height of the pillar, G_c is the work of adhesion. If we assume the height of the square and circular pillars are the same and $L=R$ the ratio of the minimum spacing w_s/w_c is

$$\frac{w_s}{w_c} = \left(\frac{\pi^4 E^* R}{2^{10} G_c} \right)^{1/6} \quad (\text{S8})$$

As the soft tip of the composite pillar is a thin layer on top of the stiff stalk, $E^*=E/(1-\nu^2)$ in eq. S8 is the plane strain modulus of the stiff stalk, which is 2.63 MPa in this study. We assume G_c is 0.2 J/m². Fig. S6 shows the ratio of the minimum spacing (w_s/w_c) as a function of the pillar radius (R). w_s/w_c decreases as R reduces, and w_s/w_c is smaller than 1 when $R < 1 \mu\text{m}$. The analysis indicates that square pillars are more favorable when the pillar size is smaller.

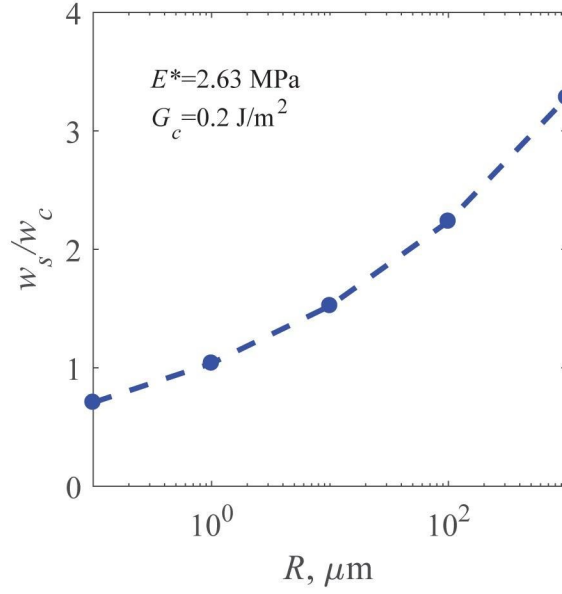


Fig. S6 Ratio of the minimum spacing w_s/w_c as a function of the pillar radius R .

Based on eqs. (S6) and (S7), the fraction of the real contact area of a pillar array to its nominal contact area can be calculated. For a square pillar array, the real contact area fraction (f_s) is

$$f_s = \frac{4L^2}{4(L + w_s)^2} \quad (\text{S9})$$

For a circular pillar array, the real contact area fraction (f_c) is

$$f_c = \frac{\pi R^2}{4(R + w_s)^2} \quad (\text{S10})$$

With $L=R$,

$$\frac{f_s}{f_c} = \frac{4(R + w_c)^2}{\pi(R + w_s)^2} \quad (\text{S11})$$

Fig. S7 shows the ratio of the real contact area fraction (f_s/f_c) as a function of the pillar radius (R) and aspect ratio (h/R). It is found that for short pillars (e.g. $h/R=2$), regardless of the pillar size, a square pillar array can always achieve higher real contact area compared to a circular pillar array.

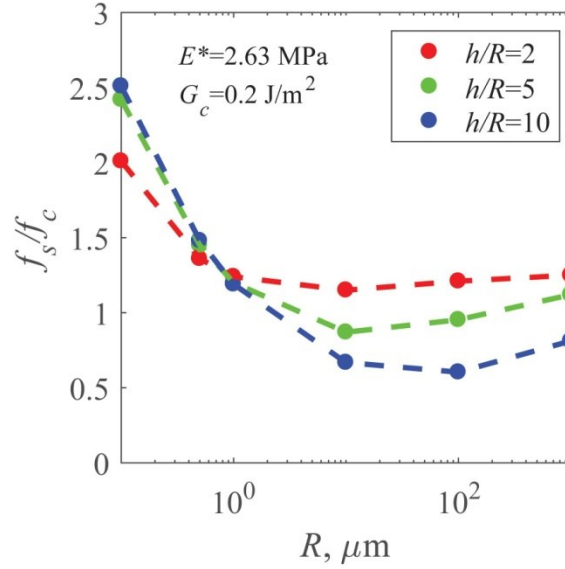


Fig. S7 Ratio of the real contact area fraction (f_s/f_c) as a function of the pillar radius (R) and aspect ratio (h/R).

Stress distributions for composite square pillars with rounded corners. Here, the FE-predicted normal stress distributions at the adhered interface for square composite pillars with rounded corners are shown.

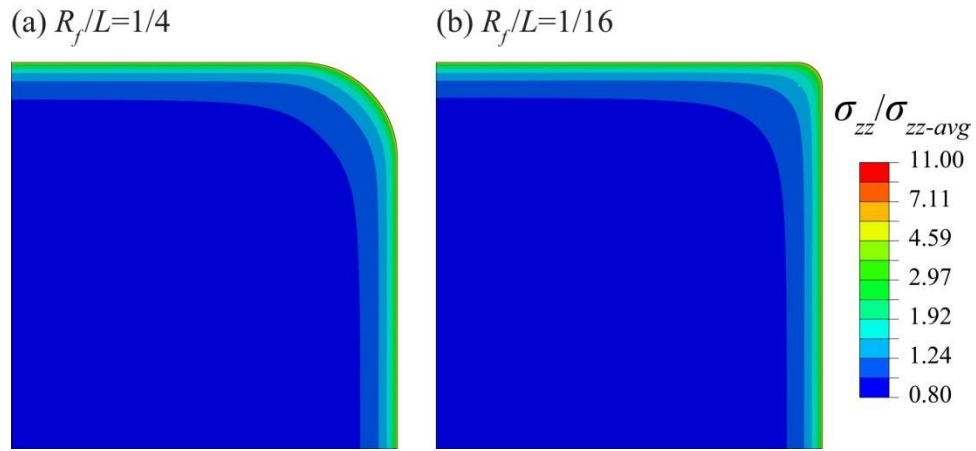


Fig. S8 Normal stress distribution at the adhered interface for a quarter-model of the square pillars with rounded corners for $t/L \geq 1.9$ (left and bottom edges are symmetry planes). Note: Color scale is logarithmic.

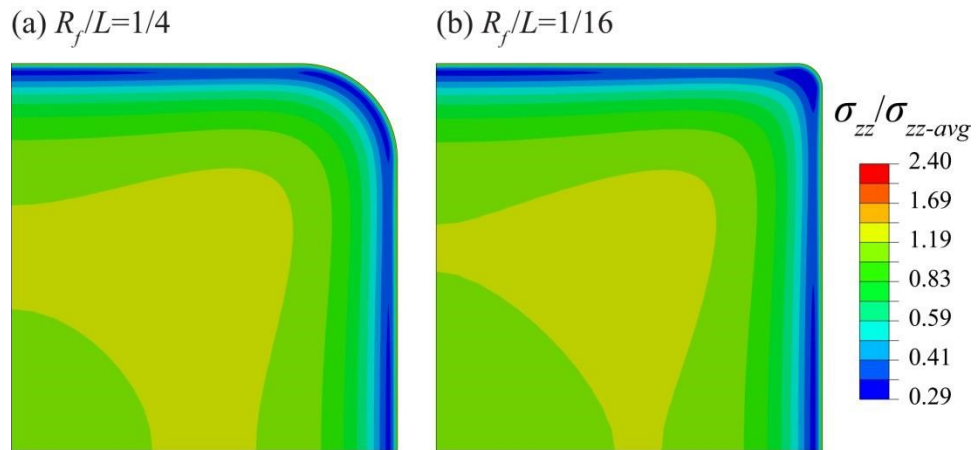


Fig. S9 Normal stress distribution at the adhered interface for a quarter-model of the square pillars with rounded corners for $t/L = 0.1$ (left and bottom edges are symmetry planes). Note: Color scale is logarithmic.

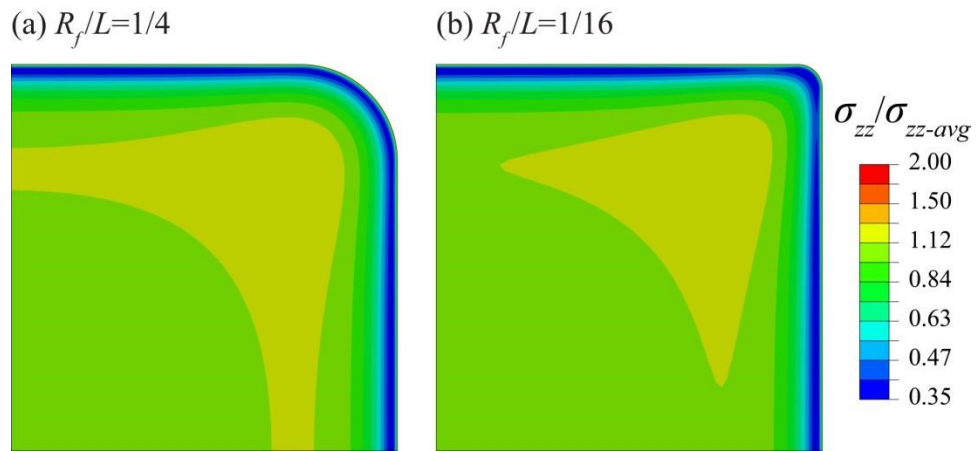


Fig. S10 Normal stress distribution at the adhered interface for a quarter-model of the square pillars with rounded corners for $t/L=0.06$ (left and bottom edges are symmetry planes). Note: Color scale is logarithmic.

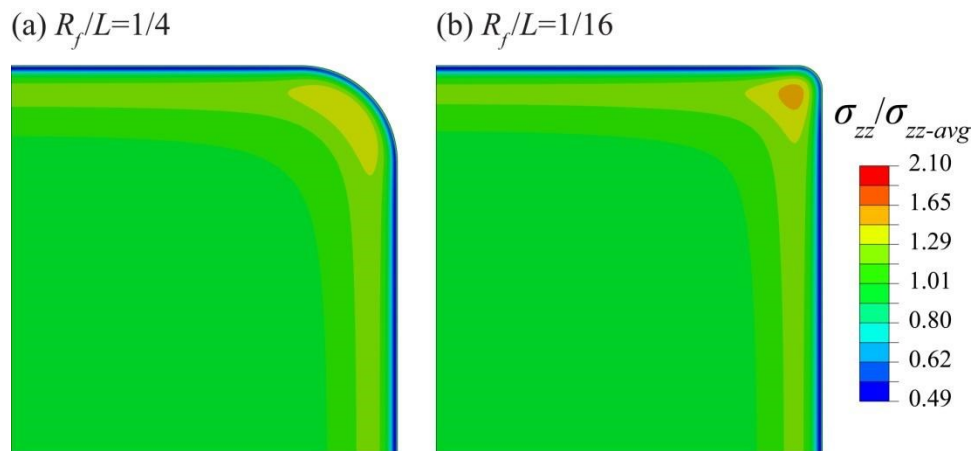


Fig. S11 Normal stress distribution at the adhered interface for a quarter-model of the pillars with rounded corners for $t/R=0.02$ (left and bottom edges are symmetry planes). Note: Color scale is logarithmic.

Dimensional analysis on the magnitude of singularity. Consider a non-dimensional stress distribution with magnitude of singularity K^* :

$$\frac{\sigma_{zz}}{\sigma_{zz-avg}} = K^* \left(\frac{r}{R} \right)^n \quad (\text{S12})$$

Rearrange:

$$\frac{\sigma_{zz}}{\sigma_{zz-avg}} = K^* R^{-n} r^n \quad (\text{S13})$$

and we have the equation in dimensional form:

$$\sigma_{zz} = K r^n \quad (\text{S14})$$

thus :

$$K = K^* \cdot (R^{-n} \cdot \sigma_{zz-avg}) \quad (\text{S15})$$

Since $n \leq 0$, given same σ_{zz-avg} applied, larger R itself results in larger K given same K^* .

References

- 1 T. L. Anderson, *Fracture Mechanics: Fundamentals and Applications*, CRC Press, Taylor & Francis Group, Fourth Edi., 2017.
- 2 M. Z. Hossain, C. J. Hsueh, B. Bourdin and K. Bhattacharya, *J. Mech. Phys. Solids*, 2014, **71**, 15–32.
- 3 P. Fratzl, H. S. Gupta, F. D. Fischer and O. Kolednik, *Adv. Mater.*, 2007, **19**, 2657–2661.
- 4 A. Luo and K. T. Turner, *J. Mech. Phys. Solids*, 2020, **143**, 104066.
- 5 N. Wang and S. Xia, *J. Mech. Phys. Solids*, 2017, **98**, 87–105.
- 6 N. J. Glassmaker, A. Jagota, C. Y. Hui and J. Kim, *J. R. Soc. Interface*, 2004, **1**, 23–33.